Journal of Engineering Physics and Thermophysics, Vol. 71, No. 6, 1998

REGULARITIES OF THE DYNAMICS OF SPHERICAL EXPLOSIONS IN HOMOGENEOUS GASES

A. M. Petrenko, G. S. Romanov,
A. N. Chumakov, and V. V. Efremov

UDC 534.222.2:621.373

It is found that the calculated recoil momentum for sufficiently large target radii is negative irrespective of the variations in the equation of state, whereas the experimentally measured value is positive regardless of the target dimensions. An explanation for the difference revealed is proposed.

The development of various methods of pulsed high-energy treatment of matter has led to the need for numerical solution of numerous problems on explosion in a homogeneous atmosphere with counterpressure. To date, considerable experience in solving these problems by various methods has been acquired [1-4]. Based on the approaches developed, one can calculate profiles of the pressure, density, mass velocity, and specific internal energy of the gas and other quantities, including the recoil momentum acting on a flat target, which is important in numerous applications. At the same time, a comparison of works [1-4] devoted to investigations of a point explosion with counterpressure revealed substantial disagreement in the calculated dependences of the specific momentum of the excess pressure on the distance to the explosion center, which are determined by the relationship

$$q_{\pm}(r) = \int_{t}^{t+\Delta t} P(r, t) - P_0)\, dt, \tag{1}$$

where P is the pressure in the shock wave, P_0 is the counterpressure (the pressure of the environment), Δt is the duration of the excess-pressure phase with a certain sign at the point r = const, and the plus and minus signs refer to the compression and rarefaction regions, respectively. Thus, in [1] the function $q(r) = q_+(r) + q_-(r)$, which is positive in the vicinity of the explosion center, first decreases with r, then becomes negative, and then increases again, still having a negative sign. In [3], $q(r)$ is negative only within a certain range of values of r. According to the results of [4], $q(r)$ is negative at large distances from the explosion center and decreases monotonically with increase in r. The agreement of the dependences $q(r)$ calculated in these works near the explosion center and the disagreement far from it can be connected with the specific features of the numerical methods applied in these works. Thus, in [1, 3] the method of a set front was used with the equation of state of an ideal gas with $\gamma = 1.4$. However, whereas in [1] this method was realized on a Lagrange grid for gas-dynamic equations in a form close to the characteristic one, in [3] the equations of gas dynamics were approximated by an explicit two-step predictor-corrector scheme on an inhomogeneous Euler grid. In [4], the method of straight-through calculation with an artificial viscosity was used, the gas-dynamic equations were approximated by the Richtmyer scheme [5] on a Lagrange grid, and the calculations were carried out for $\gamma = 1.25$.

In order to elucidate the reasons for the above discrepancies we have undertaken the present work, which is devoted to a comparison of results of numerical and experimental investigations of the momentum of recoil on a flat target in a localized contact explosion with counterpressure. We have investigated numerically the effect of variations in the equation of state on the parameters of the shock wave front (SWF), rate of transport of the explosion energy to the environment, and the recoil momentum acting on a surface located in the symmetry plane of the problem. Here, we paid special attention to the values of quantities characterizing the explosion in the late

Academic Scientific Complex "A. V. Luikov Institute of Heat and Mass Transfer of the National Academy of Sciences of Belarus," Minsk, Belarus. Translated from Inzhenerno-Fizicheskii Zhurnal, Vol. 71, No. 6, pp. 1064-1074, November-December, 1998. Original article submitted July 16, 1997.

 1062-0125/98/7106-1028$20.00

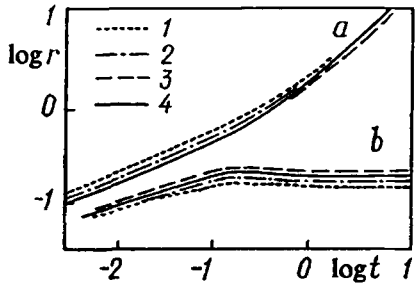

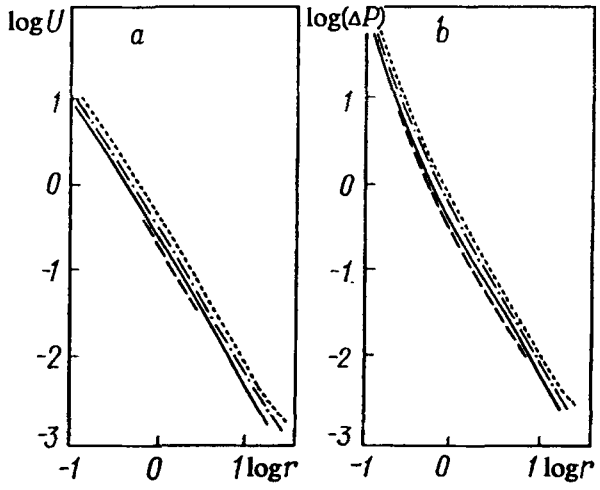

Fig. 1. Time dependences of the distance traveled by a shock-wave front (a) and the explosion source radius (b): 1) $\gamma = 5/3$, 2) 1.4, 3) 1.2, 4) air.

Fig. 2. Dependences of the amplitudes of the mass velocity (a) and the pressure excess (b) at the shock wave front on the distance of the front from the explosion center. The numbering of curves 1-4 is the same as in Fig. 1.

stages of its development – up to the instant when the pressure excess at the SWF becomes smaller than 0.2% of the counterpressure. We have also carried out experimental investigations of the recoil momentum acting on a flat target in laser break-down of air near a surface.

The problem of a spherical explosion was formulated in the form of a Cauchy problem for the gas-dynamic equations in a one-dimensional formulation with the following initial and boundary conditions. At the instant $t = 0$ the mass velocity is $U = 0$ everywhere, the density equals ρ_0 everywhere, and the pressure is $P = P_0$ outside the energy source and P_1 within the limits of the source. At the center, $U = 0$. Ahead of the SWF, $U = 0$, and the pressure and density equal P_0 and ρ_0, respectively.

The problem was considered in Lagrangian physical coordinates, which makes it possible to follow not only the SWF motion but also the development of the energy-liberation boundary. The numerical method of straight-through calculation with an artificial viscosity [5] was used to solve the problem, which is based on a completely conservative difference scheme that approximates the gas-dynamic equations up to second order of accuracy in r and t. Schemes of this type allow algebraic transformations that relate the divergent difference equation for the energy to a nondivergent one, and thus reproduce the main property of the original system of differential equations – the mutual agreement of the laws of mass, momentum, and energy conservation [6]. This is an important advantage of theirs that provides high quality of the numerical modeling. The numerical method used is implemented in the form of a software package [7] that makes it possible to carry out investigations of transient explosion-induced motion of various media.

The thermodynamics of the medium is described by the equation of state of an ideal gas. The adiabatic exponent was assumed to take values of 5/3, 1.4, and 1.2. In addition, an actual equation of state for air in tabulated form [8] was used. A uniform spatial grid was used in the calculations. At the initial instant $t = 0$ the parameters were assumed to take the following values: $P_1 = 4.777 \cdot 10^9$ Pa, $P_0 = 1.665 \cdot 10^5$ Pa for variant 1 ($\gamma = 5/3$), $P_1 = 2.8595 \cdot 10^9$ Pa, $P_0 = 10^5$ Pa for variant 2 ($\gamma = 1.4$), $P_1 = 1.4348 \cdot 10^9$ Pa, $P_0 = 10^5$ Pa for variant 3 ($\gamma = 1.2$), and $P_1 = 2.6515 \cdot 10^9$ Pa, $P_0 = 10^5$ Pa for variant 4 (air). The initial radius of the source is 10^{-3} m, the energy contained in the source is $E = 30.05$ J, and the initial density is $\rho_0 = 1.25$ kg/m^3 everywhere.

Calculated dependences of the SWF radius and the explosion-source radius on the time and of the amplitudes of the mass velocity and the pressure on the distance traveled by the wave are presented in Figs. 1 and 2. Here and in what follows, distance, time, velocity, and pressure are expressed in relative units of $\lambda = (E/P_0)^{1/3}$, $\tau = E^{1/3}\rho_0^{1/2}P_0^{-5/6}$, $C_0 = (P_0/\rho_0)^{1/2}$, and P_0, respectively. It is evident from Figs. 1 and 2 that corresponding dependences have a similar behavior for different variants. Curves corresponding to different fixed

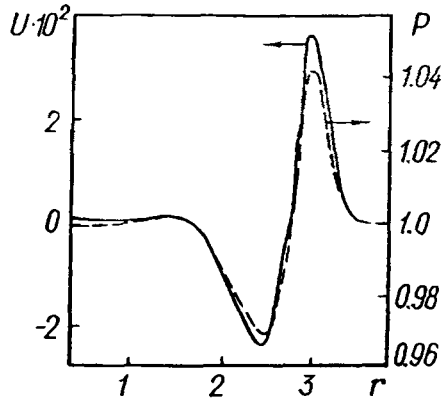

Fig. 3. Mass-velocity and pressure profiles.

γ do not cross anywhere. The only exception is the fourth variant, for which the dependences lie between the curves with $\gamma = 1.2$ and $\gamma = 1.4$. Thus, Fig. 1 shows that the trajectory of the SWF in air (curve 4) coincides with the corresponding trajectory in an ideal gas at $\gamma = 1.2$ in the early stages and with the corresponding trajectory at $\gamma = 1.4$ in the later stages. This occurs as a result of a change in the value of γ due to ionization and dissociation processes that take place in air at high pressures and temperatures. Figures 1 and 2 show an upward shift of the SWF trajectories and the time dependences of amplitude parameters that is proportional to γ. The opposite dependence on γ is observed for the position of the trajectories of the explosion-source boundary. In addition, the source is characterized by a nonmonotonic variation of the radius that has an extremum at $t \approx 0.178$ whose value is inversely proportional to γ. Then the radius decreases somewhat, and after $t \approx 1$ it finally stabilizes. The trajectory of the explosion-source boundary is determined by the dynamics of the energy transport from the source to the environment. The energy in the source reaches a minimum when its radius is maximum, then increases somewhat, which occurs as a result of motion toward the center, and finally becomes constant when the radius stabilizes. The value of this constant depends strongly on γ. The residual energy expressed in fractions of the initial energy E equals 20% for $\gamma = 1.2$, 18.4% for the variant with the tabulated equation of state, only 5.2% for $\gamma = 1.4$, and just 1.5% for $\gamma = 5/3$. This is explained by the direct dependence of the intensity of the processes of energy transport from the explosion source to the environment on γ. The higher the value of γ, the faster the source loses energy, the smaller its final size and the residual energy content, and the higher the values of the amplitude parameters of the shock wave.

Figures 1 and 2 indicate that the time dependences of the amplitude parameters of an explosion induced by an extended source differ from those for a point explosion [9]. This is best seen in Fig. 1, from which it is evident that prior to $t = 0.1$ the growth of the SWF radius and the source radius obeys a power law of the form $r = bt^{\alpha}$, $\alpha < 1$. It should be noted that b and α differ for the source and the SWF and depend on γ. Only at $t > 1$, when the source size stabilizes, does the growth of the SWF radius become linear, as in the case of a point explosion [9].

Despite the difference in calculation methods and equations of state used in the works on a point explosion with counterpressure [1, 2], in [4] and in the present work qualitatively similar pictures of the development of transient motions are revealed. Here, we deal with the three characteristic regions of the explosion-induced flow that are presented in Fig. 3 as applied to the present work. Here, the solid curve depicts a profile of the mass velocity, and the dashed curve depicts a pressure profile (variant 4, the instant of time $t = 2.14$). The first of these regions – the compression region – is formed shortly after separation of the shock wave from the boundary of the high-temperature sphere and comprises the shock-wave peak itself. It is followed by a rarefaction zone within which the mass velocity is directed toward the center and the density and the pressure have lower values than in the unperturbed medium. This zone is formed some time after the explosion, and at the beginning of its development it includes the energy-liberation region. Then the third region is formed in the center – a quiescence region [3] that expands with the SWF motion, in which the velocity is close to zero. Our calculations show that a volume explosion produces a more complicated structure of this zone. The density and the specific internal energy are

TABLE 1. Dependences of the Specific Momenta on the Radius ($q_{\pm} \cdot 10^{-2}$)

$r \cdot 10$	Air		$\gamma = 5/3$		$\gamma = 1.4$		$\gamma = 1.2$	
	$q+$	$q-$	$q+$	$q-$	$q+$	$q-$	$q+$	$q-$
0.89949	35.4676	−9.64783	51.2362	−12.6496	45.9035	−10.7834	35.6672	−8.80555
1.39529	22.3803	−9.64792	33.5666	−12.6514	28.8281	−10.7828	20.8882	−8.80551
2.37992	10.7264	−9.63516	17.6619	−12.6039	13.9303	−10.7814	8.86484	−8.8069
2.7284	8.99494	−9.57583	15.0164	−12.5274	11.4842	−10.7494	7.26799	−8.7821
3.6242	6.88038	−8.69415	10.9207	−11.9376	8.37187	−10.2466	5.76978	−7.88342
4.71725	5.71856	−7.06863	8.8121	−10.4318	6.82476	−8.66776	5.01631	−6.27639
6.05098	4.69529	−5.63748	7.17551	−8.52722	5.78857	−6.95778	4.06252	−4.98514
7.67838	3.85587	−4.50987	6.00161	−6.86549	4.74343	−5.52021	3.34118	−3.96804
9.66411	3.19532	−3.64472	4.88907	−5.55982	3.93179	−4.43897	2.73265	−3.14161
12.0871	2.54924	−2.93222	4.02276	−4.54922	3.16623	−3.57012	2.20931	−2.52594
15.0436	2.07137	−2.26572	3.26572	−3.67625	2.57349	−2.89115	1.79042	−2.04279
18.651	1.67836	−1.88876	2.65726	−2.93241	2.09081	−2.36536	1.45529	−1.68235

distributed nonuniformly within the zone. Outside the explosion source, the values of these parameters are close to their values in the unperturbed medium. Within the explosion source, the specific internal energy is substantially higher, but the density is equally lower, while the pressure in the quiescence zone is constant everywhere and equals P_0. Therefore, with development of the third region, the explosion source already does not affect the motion, despite the substantial energy content. Here, its boundary stabilizes (see Fig. 1), and the transient motion, as has been shown earlier, assumes the regime inherent in a point explosion.

The development of these regions of motion is responsible for the propelling action of the explosion, i.e., determines such parameters as the specific momentum of the excess pressure q, the total momentum J acting on a finite area, the total momentum G acting on the area involved in the motion, and the limiting momentum I acting on an area of given radius r (areas lying in the symmetry plane are assumed). The quantities J, G, and I are determined from the relationships [10]

$$J(t) = 2\pi \int_0^r \int_0^t (P - P_0)\, dtrdr,$$

$$G(t) = 2\pi \int_0^t \int_0^\infty (P - P_0)\, rdrdt, \tag{2}$$

$$I(r) = 2\pi \int_0^r \int_0^\infty (P - P_0)\, dtrdr = 2\pi \int_0^r (q_+ + q_-)\, rdr.$$

We obtained dependences of the total momenta J and G on the time and dependences of the specific momenta of the excess pressure q_+ and q_- and the limiting momentum on the area radius. Table 1 presents calculated dependences $q_+(r)$ and $q_-(r)$. Figure 4 presents dependences $G(t)$, and Fig. 5 presents dependences of the momentum $J(t)$ acting on concentric areas of radii 0.5λ, λ, and 2λ (branches a, b, and c, respectively). Figure 6 presents dependences of the limiting momentum $I(r)$. In all cases, the momentum is expressed in units of E/C_0, and q is expressed in units of $E^{1/3}\rho_0^{1/2}P_0^{1/6}$. A strong direct dependence of the quantities q, J, G, and I on γ, all other factors being the same, is evident from the figures and the table. In addition, beginning with a certain value of r that depends on γ, the absolute value of the parameter q_- becomes larger than q_+ (see Table 1). Thus, the development of the rarefaction region proves to be predominant, which agrees with results presented in [4]. This agreement means that the repeated jumps (unavoidable in the case of an extended source) that were taken into account in the

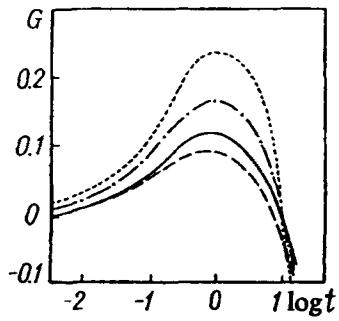

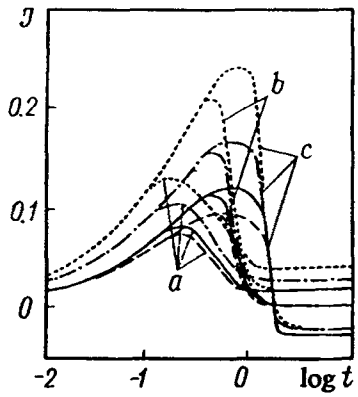

Fig. 4. Time dependence of the total recoil momentum acting on the entire plane. The numbering of curves 1-4 is the same as in Fig. 1.

Fig. 5. Time dependence of the recoil momentum acting on areas of different radii. The numbering of curves 1-4 is the same as in Fig. 4. Branches a, b, and c of the curves correspond to radii of 0.5λ, λ, and 2λ.

present work do not change qualitatively the pictures of the development of motion. It is evident from Fig. 4 that the total momentum G reaches a maximum at $t \approx 1$, then decreases, and at $t \approx 3.5$ changes sign (here the size of the area involved in the motion lies within the limits of 1.4λ to 1.9λ, depending on the value of γ). It is evident that variations in the equation of state provide a change in the maximum value of G in proportion to γ without changing its position with respect to t.

Figure 5 presents a comparison of results obtained for variants 1-4. For all the variants, the branches of the momentum J are nonmonotonic in time. Each area size r has it own maximum and upward and downward branches. Variations in the equation of state induce substantial changes in the extrema of J but virtually do not affect their position. Here the values of the extrema are directly related to γ. It is evident from the figure that the momentum J is negative at $r \approx 2\lambda$ irrespective of the variations in the equation of state, and R_c – the critical area size at which it changes sign – equals λ for air. The same figure makes it possible to trace the establishment of the limiting momentum I. It is established simultaneously for areas of the same size as a result of freezing of the total momentum J, and its value depends on γ. Since this freezing occurs as a result of expansion of the quiescence zone, the trajectory of its boundary depends only weakly on the thermodynamical properties of the medium. Figure 6 shows a strong direct dependence of the maximum of I on γ and also values of the radius at which the limiting momentum I changes its sign. The figure also illustrates a weak dependence of the position of the extremum of I on γ.

Each of the functions $G(t)$, $I(r)$, and $q(r)$ has a single maximum, upon reaching of which they monotonically decrease without limit, which indicates predominance of the rarefaction zone (see Fig. 3) in the late stage of the explosion. A similar predominance of the rarefaction zone has also been revealed in [1, 2, 4, 10] (the results of [3] do not allow for a concrete conclusion). Thus, virtually all known calculations of a spherical explosion with counterpressure carried out by various numerical methods using various equations of state yield, irrespective of the method of representation of the energy source (point or extended, instantaneous or time-dependent), one and the same qualitative result – predominance of the rarefaction region of the explosion-induced flow at long scatter times.

This theoretical result has an experimental substantation. In [11, 12], dependences of the recoil momentum of the laser-induced breakdown of air on the target dimensions were presented: for a flat target and a hemisphere (breakdown at the center of curvature). A nonmonotonic behavior of this quantity has been revealed – growth with the target size is followed by attainment of a maximum and a decrease. The information presented above means that the predominance of the rarefaction region in an explosion-induced flow is a consequence of the laws of mass, momentum, and energy conservation. This is one of the main features of spherical shock wave motion under conditions of counterpressure. A second interesting feature is the absence of a phase shift between the pressure and velocity profiles (Fig. 3).

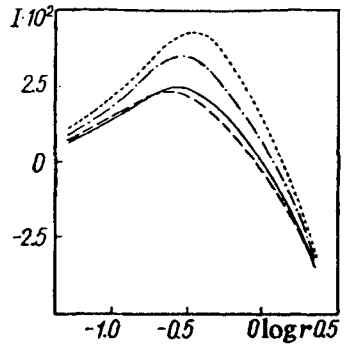

Fig. 6. Dependence of the limiting recoil momentum on the target radius. The numbering of curves 1-4 is the same as in Fig. 1.

Since the results in [11, 12] were obtained for small targets for which the recoil momentum is still positive, we carried out similar experiments with very large targets. Inasmuch as fabrication of light and durable targets with a radius exceeding 0.1 m presents difficulties, we had to give up the idea of carrying out experiments with an explosion energy similar to that used in the calculations $E = 30.05$ J, and the experiments were carried out at the energy $E = 0.1$ J. Since the solution to the problem of an explosion with counterpressure is not self-similar [13], the above numerical results cannot be compared with results of experiments obtained for a substantially differing energy. Therefore, we additionally carried out calculations for the problem of an explosion in the same formulation with initial parameters corresponding to the experiment (see below). The initial source radius was $0.1 \cdot 10^{-3}$ m, the source energy was $E = 0.2$ J (due to the spherical symmetry of the problem). The unit of length in this case is $\lambda = 10^{-2}$ m. The equation of state of an ideal gas with $\gamma = 1.4$ was used. The calculations yielded results qualitatively similar to those presented above and therefore they will not be described here. We should only mention that the equality $R_c = \lambda$ also holds in this case.

Near-surface optical breakdown of air induced by laser radiation acting on the surface of a metal target at the atmospheric pressure was used as the local explosion. A laser setup [14] based on a pulsed-periodic Nd^{3+} YAG laser operating in the Q-switching mode was used in the experiments. The bell-shaped laser pulse (a wavelength of 1.064 μm) had a duration of $2 \cdot 10^{-8}$ sec and an energy of 0.1 J. The laser radiation was focused on the target surface by a planoconvex spherical lens with a focal length of 60 mm. The diameter of the homogeneous radiation spot was 200 μm. The laser-radiation fluence was varied in the experiments by means of glass light filters within the range of 0.1–12 GW/cm^2.

The dynamics of near-surface optical breakdown and the properties of near-surface plasma plumes appearing under the given conditions of laser action have been described in detail elsewhere [15]. At a laser-radiation fluence $w > 0.3$ GW/cm^2, transfer of a plasma front into air takes place, and its propagation occurs in the mode of light-induced detonation. When the laser-radiation fluence is increased to 1 GW/cm^2, radiation processes of the plasma-front transfer begin to play an important part in forming near-surface plasma plumes, and they become dominating at $w > 4$ GW/cm^2 irrespective of the target material. Under these conditions near-surface plasma plumes are spindle-shaped. However, even at $w = 12$ GW/cm^2 their dimensions do not exceed 2 mm. By the end of the laser pulse and upon separation of the shock wave from the plasma front, the two-dimensional character of the gas-dynamic scattering becomes progressively less pronounced, and at distances that exceed the size of the near-surface plasma plume by an order of magnitude, the shock wave can be considered to a good approximation as having a hemispherical shape.

Subsequently, the region occupied by the near-surface plasma plume transforms into a low-density high-temperature sphere floating up along the vertically oriented target surface (see below) under the action of the Archimedes force and the viscosity. Inasmuch as the axial symmetry of the motion is broken in this case, the development of the perturbation already cannot be modeled by a one-dimensional calculation. However, estimates show that in the time necessary for the shock wave to travel a distance of 12λ the sphere shifts by just $0.5 \cdot 10^{-3}\lambda$, and therefore its motion in these experiments can be neglected. At the initial instant, the region of the near-surface plasma plume appears to be filled with an ionized gas and metal vapor, and the energy is distributed

inhomogeneously over the region. This differs from the initial conditions in the source used in our calculations. They equations of state used in this work did not take metal vapor into account. However, as has been noted above, the alternating-sign character of the recoil momentum is not determined by the thermodynamics of the medium. In the calculations, we did not take into account the component of the recoil momentum due to evaporation of the target material. However, it is evident that taking this component into account will result in a shift of the curves $G(t)$, $J(t)$, and $I(r)$ (Figs. 4-6) upward, and their zeros will shift to higher values. In other words, additional components of the recoil momentum will just provide an increase in R_c. Estimates based on the initial parameters of a calculation for an aluminum target show that $R_c \approx 1.6\lambda = 1.6 \cdot 10^{-2}$ m when evaporation is taken into account.

Finding a critical target size for which the recoil momentum changes sign was one of the objectives of the experimental investigation. To do this, two series of experiments with different targets were carried out. In the first series, a disk of aluminum foil with a radius of $1.5 \cdot 10^{-2}$ m was used as the target. This disk was attached to a lever mounted on a vertical needle using a ruby bearing so as to provide its free rotation about a vertical axis. The lever was balanced by an identical disk attached to its opposite end. At the initial instant, the target plane was oriented normal to a horizontally propagating laser beam aimed at its center. According to results of calculations, positive recoil momentum directed along the beam was expected for target radii $r < R_c$, and positive recoil momentum in the opposite direction was expected for $r > R_c$. The direction of the lever motion should change accordingly. Experiments with this target showed that the recoil momentum is positive.

The second series of experiments was carried out with a target of radius $r = 5 \cdot 10^{-2}$ m. It was made of dense paper and was suspended by means of two vertically spaced paper supports on a vertically stretched thread, and it rotated freely about the thread. The rotation radius was $6 \cdot 10^{-2}$ m. An aluminum foil disk was attached to the center of the target in the region of formation of the near-surface plasma plume. In this case, a positive sign of the recoil momentum was also found. Thus, the propellant effect does not change its sign. Upon further increase in the target radius r, the velocity of its motion decreases as r^{-2} as a result of the increase in mass.

Effects connected with streamlining of the target edges reduce the recoil momentum but cannot provide a constant sign of the momentum. In addition, the gas flows to the region behind the target from the region with increased pressure, which is followed by a rarefaction zone. A counterflow proceeds into the latter. This motion cannot extend itself outside the rarefaction zone, since the pressure in the quiescence zone equals that in the unperturbed medium. Most likely, these counterflows, having opposite effects on the target motion, cancel each other out, since the use of a special panel hampering the gas flow to the region behind the target had no effect on the results obtained.

The experiments have revealed the strictly positive sign of the recoil momentum independently of the target size. This means that a qualitative disagreement between the results of numerical calculations of the explosion with counterpressure and the experiment occurs for scattering times $t > 1$. This can be explained by some physical process not taken into account that is involved at small values of the parameters of the SWF and reduces the steepness of the pressure profile in the compression zone and substantially enhances it in the rarefaction zone and thus provides a balance of the contributions of these regions to the recoil momentum. In our calculations, we did not take into account dissipation processes due to the viscosity and the thermal conductivity or relaxation processes, which provide the existence of a second viscosity in polyatomic gases [16]. However, both the viscosity and the thermal conductivity provide a decrease in the steepness of the pressure profile in all regions of motion [17]. In addition, estimates made for the case of a spherical explosion in a heat-conducting viscous gas [18] show that the ratio of dissipative terms to inertial terms in the Navier–Stokes equations decreases with increase the arrival time of the shock wave as t^{-1} for the region far from the explosion center and as $t^{-1+3/(\gamma+2)}$ for the region close to the explosion center. Therefore, dissipation processes exert a substantial direct effect on the development of transient motions only in the vicinity of the explosion center for short scattering times. It is thus evident that these processes cannot explain the disagreement between the experiment and the results of the calculations.

Relaxation processes provide the frequency dependence of the phase velocity of sound (dispersion) provided that the frequency of sound $\nu > 1/t_r$, where t_r is the relaxation time. In a medium with dispersion, the evolution of any perturbation with a finite amplitude is determined by the relative contributions of effects of the nonlinear interaction of its Fourier components and dispersion effects. The latter lead to transformation of the perturbation

into a broadening wave packet. Nonlinear effects characterized by the Mach number M provide transport of the perturbation energy to higher frequencies and thus provide its stability. The interrelationship of the above effects is characterized by the parameter [19]

$$D = \frac{2(C_D^2 - C^2)}{\pi M C^2 (\gamma + 1)}, \tag{3}$$

where C and C_D are the velocities of sound in media without and with dispersion, respectively.

Dispersion is always neglected in the physics of explosion. This occurs because no dispersion is observed in all homogeneous media with low absorption of sound [20]. In gases, dispersion is observed within the narrow frequency range of 10–100 kHz [21], in which absorption is high. On the other hand, in the near and middle explosion zones, having primary importance in explosion experiments and technologies, the amplitude values of the Mach number M are high, so that $D \ll 1$. In these regions, the evolution of the shock-wave peak is determined by dissipation processes, which, along with relaxation processes, provide growth of its width and an additional decrease in its amplitude with increase in the distance from the explosion center.

In the far explosion zone, which in the case under consideration corresponds to a scattering time $t > 1$, a different picture is observed. Neglecting dispersion effects is already unjustified. However, here only qualitative estimates can be made, since no theory of the acoustical dispersion has been developed. It should be noted that the effect of dissipation processes becomes small as a result of a substantial decrease in the amplitude parameters of the perturbation front [18]. The amplitude Mach number acquires the value M_D at which $D \approx 1$, i.e., the contributions of dispersion and nonlinear effects cancel each other out. Here, dispersion is already a decisive factor affecting the evolution of the perturbation peak, whose effect results in rapid growth of the peak width with decreasing M. The dispersion-induced broadening of the rarefaction zone is substantially smaller, since, due to the fact that it has a substantially larger width, the contribution of high-frequency Fourier components, which undergo dispersion, is relatively small here. As a result, the contributions of the compression and rarefaction regions to the recoil momentum cancel each other out. Finally, when $D > 1$, the interaction of Fourier components of the perturbation becomes so negligible that the superposition principle appears to be applicable to them. Since the velocities of these components are different, the perturbation transforms into a broadening sound-wave packet. Its high-frequency components are rapidly absorbed, whereas low-frequency components propagate to great distances from the location of the explosion, i.e., dispersion leads to transformation of the shock-wave motion into an acoustic perturbation. Here the amplitude value of the Mach number M_D restricts the stability region of the shock wave from below.

It has been shown in [22] that in the case of an acoustic perturbation the time-averaged deviation of the pressure from its equilibrium value equals zero in all space. In the same work, the following relationship for this quantity has been derived:

$$\int_0^\infty (P - P_0)\, r dr = 0,$$

from which is evident that an acoustic perturbation does not contribute to the recoil momentum. Therefore, after the above transformation the recoil momentum has a constant residual value whose magnitude and sign depend on the number M_D. Our experiments show that this value is positive for air at NTP.

In the case of spherical symmetry, an acoustic wave differs from a shock wave by a phase shift between the pressure and velocity profiles [23] that decreases with increase in the distance from the origin. Relaxation processes can provide this shift, since they lead to a delay in establishment of equilibrium with respect to the pressure change and, therefore, to a phase shift between the pressure and the internal energy [24].

With the development of the dispersion-induced instability, the perturbation region can be represented as a pulsed isotropic acoustic source with the maximum of the spectral radiation density corresponding to the frequency $\nu \approx R_D/C$, where R_D is the radius of the perturbation region at $M = M_D$. Vibrations with this frequency propagate

to great distances from the location of the explosion. By using the graphical data presented above, one can represent the period of these vibrations within the approximation of the instantaneous transformation of the shock wave into an acoustic perturbation as follows:

$$T = \eta\gamma^{-(\sigma+1)/2} M_D^{-\sigma} E^{1/3} \rho_0^{1/2} P_0^{-5/6}. \quad (4)$$

Relationship (4) has been derived with regard for the fact that the dependence of the mass-velocity amplitude on the front radius (Fig. 2a) is well approximated by a power law within the range of $1 < r < 10$. $\eta = 0.8934$ and $\sigma = 0.564$ for $\gamma = 5/3$, $\eta = 0.783$ and $\sigma = 0.552$ for $\gamma = 1.4$, $\eta = 0.6513$ and $\sigma = 0.531$ for $\gamma = 1.2$, and $\eta = 0.712$ and $\sigma = 0.536$ for real air. If one assumes that air corresponds to an ideal gas with $\gamma = 1.25$ in the late scattering stage, and the transformation takes place instantaneously at the instant of time corresponding to the inflection point in Fig. 5 (branch c for air), one obtains $T = 5.963 \cdot 10^{-4}$ sec from (4). The value $M = 6.86 \cdot 10^{-2}$, which is assumed to be close to the threshold value M_D, corresponds to this point.

The following empirical relationship for evaluating the period of infrasound vibrations induced by a near-surface nuclear explosion in the atmosphere is presented in [25]:

$$T \approx 4 \cdot 10^{-4} (E/4.2)^{1/3} \quad (5)$$

(here and in (4) T is expressed in seconds). For the energy $E = 30.05$ J, Eq. (5) yields the value $T = 6.118 \cdot 10^{-4}$ sec. The closeness of these two values of T serves as an indirect substantiation of the above concepts. However, the small difference (2.5%) may well be due to accidental mutual compensation of errors in gas-dynamic calculations of the shock wave at the stability threshold on the one hand and errors in extrapolating estimates valid for a high-energy explosion to a low-energy explosion due to the non-self-similar character of the problem on the other hand.

Since in this case the acoustic signal has no other energy sources except for internal motions within a region of radius R_D, its duration can be estimated as $\Delta T \sim R_D/C$. Then, by using the uncertainty principle [26] according to which the width of the spectrum of a signal ΔH and its duration obey the relationship $\Delta H \Delta T = \text{const}$, we obtain the following estimate for the spectrum width far from the explosion giving rise to the signal: $\Delta H \sim E^{-1/3} \times \times \rho_0^{-1/2} P_0^{5/6}$. Thus, the spectral characteristics of acoustic radiation due to a shock wave are unambignously related to the explosion energy, the equilibrium values of pressure and density, and the thermodynamic and dispersion properties of the medium.

It follows from Eq. (3) that with a change in the contribution of dispersion effects, one observes changes in the threshold Mach number M_D, which most likely is an individual characteristic of each acoustic medium, since all media differ by relaxation processes giving rise to dispersion. Thus, in monatomic gases at NTP, one observes translational dispersion [21] due to relaxation of the deviation of the velocity distribution function from the Maxwell distribution and due to fluctuations. In polyatomic gases under the same conditions one also observes rotational dispersion due to processes of energy redistribution between internal rotational degrees of freedom. This makes it possible to suppose that M_D is smaller in monatomic gases than in polyatomic ones. In the case of inert gases an increase in M_D with the molecular weight of the gas should be expected, since the average time of existence of fluctuations is proportional to the molecular weight. If this is so, then helium is characterized by the minimum M_D and the minimal frequency of the main component of the explosion-induced acoustic signal, all other conditions being the same. Most likely, the sign-varying character of the recoil momentum, whose absence in air has been established in the present work, is possible in inert-gas atmospheres. This problem thus requires further experimental and theoretical investigations.

CONCLUSIONS

1. Results of numerical gas-dynamic simulations of transient explosion-induced symmetrical gas motions agree qualitatively with experiments within the (bounded from below) region of amplitude Mach numbers $M > M_D$,

when nonlinear effects dominate over dispersion. Outside this region, the gas-dynamic description of transient motions becomes inapplicable, since it leads to negative values of the calculated recoil momentum for certain target sizes, whereas the experimentally measured recoil momentum is positive irrespective of the target size.

2. The qualitative disagreement of theoretical and experimental results stems from the fact that dispersion of sound, which limits the region of existence of a shock wave and leads to transformation of shock-wave motion into an acoustic perturbation, is not taken into account in the calculations. It should be noted that in actual media, the stability region of a shock wave is determined by the condition $M > M_D$. However, in an ideal medium with dissipation but without dispersion (i.e., $M_D = 0$) transient explosion-induced motion takes place only in the form of a shock wave. In this case the gas-dynamic description of an explosion leads to correct results without restrictions.

3. The parameters of the acoustic signal induced by an explosion in a gas are related to the explosion energy, the counterpressure, the equilibrium gas density, and its thermodynamic and dispersion properties. This makes it possible to consider an explosion in a gas not only as a pulsed acoustic source with a spectrum that is tunable over a wide range but also as a means of investigation of acoustic dispersion.

The authors thank L. Ya. Min'ko for support of the work.

NOTATION

q, specific momentum of excess pressure; r, dimensionless distance; γ, adiabatic exponent; U, dimensionless mass velocity; E, explosion energy; ρ_0, initial density of the medium; λ, unit distance; τ, unit time; C_0, unit velocity; b and α, constants of the power law of motion of the shock wave and the boundary of the explosion source; J, total recoil momentum acting on a bounded area; G, total recoil momentum acting on the entire plane; I, limiting recoil momentum; R_c, critical target size at which the recoil momentum changes sign; w, laser-radiation fluence; ΔP, pressure jump on the shock-wave front; M, amplitude Mach number; D, parameter characterizing the ratio of nonlinear and dispersion effects; T, period of acoustic vibrations propagating to large distances from the explosion location; η, coefficient in the equation defining T; σ, exponent of the power law of the dependence of T on the threshold value of the Mach number M_D that determines the stability regionof the shock wave; ΔI, duration of acoustic radiation; ΔH, width of the acoustic-radiation spectrum.

REFERENCES

1. D. E. Okhotsimskii, I. L. Kondrasheva, Z. P. Vlasova, and R. K. Kozakova, Trudy Matem. Inst. Akad. Nauk SSSR, 50, 3-65 (1957).
2. D. E. Okhotsimskii and Z. P. Vlasova, Zh. Vychisl. Matem. Matem. Fiz., 2, No. 1, 107-124 (1962).
3. Kh. S. Kestenboim, G. S. Roslyakov, and L. A. Chudov, Point Explosion: Methods of Calculation and Tables [in Russian], Moscow (1974).
4. G. Brode, in: Mekhanika, Novoe v Zarubezhnoi Nauke, Moscow, No. 4 (1976), pp. 7-70.
5. R. Richtmyer and C. Morton, Difference Methods of Solving Boundary-Value Problems [Russian translation], Moscow (1978).
6. A. A. Samarskii and Yu. P. Popov, Difference Methods of Gas Dynamics [in Russian] (1975).
7. A. M. Petrenko, Algoritmy i Programmy. Informatsionnyi Byulleten', No. 11, 4 (1988).
8. N. M. Kuznetsov, Thermodynamic Functions and Shock Adiabats of Air at High Temperatures [in Russian], Moscow (1965).
9. V. P. Korobeinikov, Problems of Point Explosions [in Russian], Moscow (1986).
10. I. N. Kovaleva and I. V. Nemchinov, Fiz. Goreniya Vzryva, 12, No. 1, 113-116 (1976).
11. N. I. Kozlova, A. N. Petrukhin, Yu. E. Pleshanov, V. A. Rybakov, and V. A. Sulyaev, Fiz. Goreniya Vzryva, 11, No. 4, 650-654 (1975).
12. F. V. Bunkin and A. M. Prokhorov, Uspekhi Fiz. Nauk, 119, Issue 3, 425-446 (1976).
13. L. I. Sedov, Similarity and Dimensional Methods in Mechanics [in Russian], Moscow (1977).

14. V. V. Efremov, N. A. Tylets, A. N. Chumakov, and Yu. F. Shienok, Pribory Tekhn. Éksperim., No. 4, 179-183 (1992).
15. A. N. Chumakov, V. V. Efremov, N. A. Bosak, L. Ya. Min'ko, Yu. A. Chivel', and V. B. Abramenko, Kvant. Élektron., 21, No. 8, 773-777 (1994).
16. L. I. Mandel'shtam and M. A. Leontovich, Doklady Akad. Nauk SSSR, 3, No. 3, 110-114 (1936).
17. Ya. B. Zel'dovich and Yu. P. Raizer, Physics of Shock Waves and High-Temperature Hydrodynamic Phenomena [in Russian], Moscow (1966).
18. V. V. Sychev, Prikladn. Matem. Mekh., 29, Issue 6, 997-1003 (1975).
19. O. V. Rudenko and S. I. Soluyan, Theoretical Foundations of Nonlinear Acoustics [in Russian], Moscow (1975).
20. E. A. Zabolotskaya, Trudy FIAN, 156, 31-41 (1984).
21. I. G. Mikhailov, V. A. Solov'ev, and Yu. P. Syrnikov, Principles of Molecular Acoustics [in Russian], Moscow (1964).
22. L. D. Landau and E. M. Lifshits, Hydrodynamics [in Russian], Moscow (1986).
23. É. V. Lavrent'ev and O. I. Kuzyan, Explosion in the Sea [in Russian], Leningrad (1977).
24. B. B. Kudryavtsev, Ultraacoustic Methods of Investigation of Substances [in Russian], Moscow (1961).
25. G. A. Bush, A. I. Grachev, S. N. Kulichkov, A. K. Matveev, M. I. Mordukhovich, and A. I. Otrezov, Propagation of Infrasound Waves Induced by an Experimental Explosion [in Russian], Moscow (1982).
26. J. Bendat, Theory of Random Noise and Its Applications [Russian translation], Moscow (1965).